THE JOURNAL OF PHYSICAL CHEMISTRY B

Article

pubs.acs.org/JPCB

Interaction of Magnesium Ions with Pristine Single-Layer and Defected Graphene/Water Interfaces Studied by Second Harmonic Generation

Jennifer L. Achtyl,[†] Ivan V. Vlassiouk,[‡] Sumedh P. Surwade,[§] Pasquale F. Fulvio,[§] Sheng Dai,[§,∥] and Franz M. Geiger*[,†]

[†]Department of Chemistry, Northwestern University, 2145 Sheridan Road, Evanston, Illinois 60208, United States

[‡]Measurement Science & System Engineering Division, Oak Ridge National Laboratory, Oak Ridge, Tennessee 37931, United States

[§]Chemical Sciences Division, Oak Ridge National Laboratory, Oak Ridge, Tennessee 37831, United States

[∥]Department of Chemistry, University of Tennessee, Knoxville, Tennessee 37996, United States

Supporting Information

ABSTRACT: This work reports thermodynamic and electrostatic parameters for fused silica/water interfaces containing cm^2-sized graphene ranging from a single layer of pristine graphene to defected graphene. Second harmonic generation (SHG) measurements carried out at pH 7 indicate that the surface charge density of the fused silica/water interface containing the defected graphene (−0.009(3) to −0.010(3) C/m^2) is between that of defect-free single layer graphene (−0.0049(8) C/m^2) and bare fused silica (−0.013(6) C/m^2). The interfacial free energy of the fused silica/water interface calculated from the Lippmann equation is reduced by a factor of 7 in the presence of single-layer pristine graphene, while defected graphene reduces it only by a factor of at most 2. Subsequent SHG adsorption isotherm studies probing the Mg^{2+} adsorption at the fused silica/water interface result in fully reversible metal ion interactions and observed binding constants, K_{ads}, of 4(1) − 5(1) × 10^3 M^{-1} for pristine graphene and 3(1) − 4(1) × 10^3 M^{-1} for defected graphene, corresponding to adsorption free energies, ΔG_{ads}, referenced to the 55.5 molarity of water, of −30(1) to −31.1(7) kJ/mol for both interfaces, comparable to Mg^{2+} adsorption at the bare fused silica/water interface. Maximum Mg^{2+} ion densities are obtained from Gouy−Chapman model fits to the Langmuir adsorption isotherms and found to range from 1.1(5) − 1.5(4) × 10^{12} ions adsorbed per cm^2 for pristine graphene and 2(1) − 3.1(5) × 10^{12} ions adsorbed per cm^2 for defected graphene, slightly smaller than those of for Mg^{2+} adsorption at the bare fused silica/water interface ((2−4) × 10^{12} ions adsorbed per cm^2), assuming the magnesium ions are bound as divalent species. We conclude that the presence of defects in the graphene sheet, which we estimate here to be around 1.3 × 10^{11} cm^2, imparts only subtle changes in the thermodynamic and electrostatic parameters quantified here.

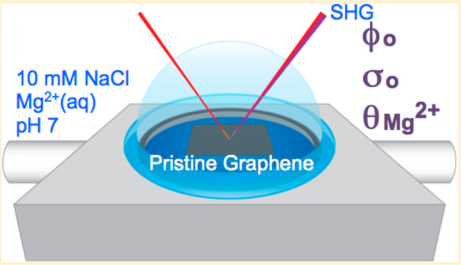

I. INTRODUCTION

Research on graphene has grown almost exponentially since the isolation of single layer graphene by Novoselov and Geim in 2004/5.[1−3] Graphene has garnered much interest due to its mechanical, electronic, magnetic, thermal, and optical properties, which have led to the utilization of graphene in numerous applications, including energy conversion and storage, separation, sensing, biomedicine, catalysis, and material science.[4−13] Recent reviews and articles have emphasized the need to expand fundamental studies of bare graphene, functionalized graphene, and other carbon substrates, as knowledge gleaned from such studies is necessary in order to understand, control, improve, and realize the various graphene applications.[3,5,14] Many of these envisioned applications involve graphene at a fluid−solid interface.[13,15−21] However, fundamental investigations of graphene located in such an interfacial environment have been curtailed by the difficulty in (a) accessing the liquid/graphene/substrate interface and (b) reliably producing pristine single layer graphene sheets large enough for spectroscopic probes. As such, most adsorption studies over graphene have been restricted to the experimental methods of ultrahigh vacuum deposition and electron beam vapor deposition methods,[22−24] or to theoretical studies.[2,25−27]

Here, we overcome these challenges by using chemical vapor deposition (CVD)[2,14,15,28] to prepare cm^2-sized graphene samples ranging from pristine single layers to defected multilayers, and probing their interaction with electrolytes at fused silica/water interfaces via second harmonic generation (SHG). We track adsorption/desorption processes in real time, in situ, under aqueous flow conditions, and without the necessity of having to use electrochemical or spectroscopic

Special Issue: James L. Skinner Festschrift

Received: October 17, 2013
Revised: February 6, 2014
Published: February 11, 2014

   dx.doi.org/10.1021/jp410298e | J. Phys. Chem. B 2014, 118, 7739−7749

labels. Moreover, we provide interfacial charge densities, interfacial potentials, free energies of binding, and observed binding constants for graphene, having various degrees of defects, upon interaction with Mg(II) ions adsorbing from aqueous solution maintained at pH 7 and 10 mM ionic strength. While the interaction of Mg(II) ions with carbon substrates is relevant for applications in metal ion secondary batteries, magnesium−air fuel cells, and nanoelectronics,[10,20,25] Mg(II) also exhibits straightforward aqueous bulk speciation and serves as a foundation for expanding our studies with other divalent and trivalent cations, including rare earths.

The results from this study will serve as a benchmark for future experimental and theoretical work. Furthermore, our work addresses recent calls for further investigation regarding the identification and effect of graphene defects,[1,2,5,14,16] the role of the supporting substrate,[1,5] the development of standardized methods for surface characterization,[2,29] and for the development of experimental techniques suitable for tracking processes occurring at fluid/solid interfaces in situ, over relevant substrates, and under the relevant experimental conditions.[2,16,20,25]

II. BACKGROUND

A. The Eisenthal $\chi^{(3)}$ Technique. Previous SHG studies of graphene and graphitic films have focused on SHG signal as a function of sample azimuthal angle and bias electric current/field in graphene,[30−34] and additional third-order nonlinearities of graphene films have been explored,[35−40] yet, to our knowledge, SHG studies addressing how ions adsorb to graphene from aqueous solution have not been published. SHG is a coherent nonlinear optical spectroscopy that is highly sensitive to the structure and thermodynamics of interfaces.[41−43] Second harmonic signal arises when two photons of one frequency, ω, combine to create a photon of frequency 2ω. The intensity of the second harmonic response is a function of the second and third nonlinear susceptibilities, $\chi^{(2)}$ and $\chi^{(3)}$, of the interface given by

$$I_{SHG} \propto |E_{SHG}|^2 \tag{1a}$$

$$E_{SHG} \propto P_{2\omega} = \chi^{(2)} E_\omega E_\omega + \chi^{(3)} E_\omega E_\omega \Phi_0 \tag{1b}$$

where I_{SHG} and E_{SHG} are the SHG signal intensity and E-field, respectively, $P_{2\omega}$ is the induced second order polarization, E_ω is the incident electric field at frequency ω, and Φ_0 is the interfacial potential.[41,44−48] Contributions to the $\chi^{(2)}$ term originate from a break of centrosymmetry at the interface, including the adsorption of analytes on resonance with the incident electric field.[42−44,49,50] Contributions to the $\chi^{(3)}$ term originate from the reorientation and polarization of water molecules aligned by a static electric field.[41,47,50−52] A charged interface, like that of fused silica at pH 7,[53] will set up a static E-field, which induces an interfacial potential that decays into the bulk over a distance characterized by the Debye length.[54−56] If the incident E-field does not match an electronic resonance of a surface-localized species, I_{SHG} will be dominated by the third-order term. As such, we can use the $\chi^{(3)}$ technique, pioneered by Eisenthal and co-workers,[46−48] to track magnesium adsorption at the graphene interface by measuring changes in the second harmonic signal intensity, which is modulated by changes in the interfacial potential due to the presence of the counterions.

In the $\chi^{(3)}$ technique, the second harmonic intensity can be expressed as a function of the interfacial potential:[47]

$$E_{SHG} \propto P_{2\omega} = A + B\Phi_0 \tag{2}$$

Here, the A and B are parameters composed of constants, including the susceptibilities and E-fields from eq 1. It is assumed that there is a relative phase of zero between $\chi^{(2)}$ and $\chi^{(3)}$ and that under the conditions of this experiment, the $\chi^{(2)}$ term remains constant, and the incident electric field and nonlinear susceptibility constants do not change. An in-depth analysis of these assumptions is available in a previous publication covering the sensitivity of the $\chi^{(3)}$ method.[56] In this sensitivity analysis, we reported SHG signal detection limits as low as $10^{-7} - 10^{-8}$ V with 0.3 μJ input pulse energy.[56] As evident by eq 2, a decrease of the SHG intensity can be attributed to a decrease in the interfacial potential due to charge screening caused by the adsorption of counterions. Tracking the change of I_{SHG} with increasing electrolyte concentration can produce valuable interface specific parameters, such as surface charge density, interfacial potential, and subsequently thermodynamic binding parameters. By applying an appropriate surface complexation model, the $\chi^{(3)}$ method has been successfully utilized to determine these important interface specific parameters for a variety of systems including oxides,[48,51,53,56−73] DNA,[74−82] and lipid bilayers.[83]

B. The Diffuse Layer Model. The Gouy−Chapman equation, given by eq 3, is a common electrical double layer theory used to model interfacial potential as a function of net surface charge density (σ) and total electrolyte concentration (C_{elec}).[54,55,84,85]

$$\Phi_0 = \frac{2k_BT}{ze} \sinh^{-1}\left[\sigma \sqrt{\frac{\pi}{2\varepsilon\varepsilon_0 T C_{elec}}}\right] \tag{3}$$

Here, z is the charge of the screening electrolyte, e is the charge of an electron, ε is the dielectric constant of water at 25 °C, ε_0 is the permittivity in a vacuum, k_B is the Boltzmann constant, and T is temperature. The SHG intensity can be expressed as a function of surface charge density and bulk electrolyte concentration by combining eqs 2 and 3.

$$|E_{SHG}| \propto A + B * \sinh^{-1}\left[(\sigma)\frac{30.2\ \mathrm{M}^{1/2}\ \mathrm{m}^2\ \mathrm{C}^{-1}}{\sqrt{C_{elec}}}\right] \tag{4}$$

By executing a "charge screening" experiment we can determine the initial surface charge density.[53,56,59,64,86] For this experiment the SHG response is measured at constant pH and as a function of increasing electrolyte concentration where a change in I_{SHG} is due to the screening of interfacial charges. The resulting charge screening curve is then fit with eq 4 to yield the initial surface charge density, σ_0, which is then used as a constraint to determine thermodynamic adsorption parameters for Mg(II) adsorption. In this case, the second harmonic signal is measured at constant ionic strength and bulk pH and as a function of bulk metal ion concentration, and the net surface charge density, σ, is expressed as the sum of the initial surface charge density of the substrate, σ_0, and any additional charge due to the adsorbed species at monolayer coverage, σ_m, multiplied by a Langmuir expression according to[52]

$$\sigma = \sigma_0 + \sigma_m\left(\frac{K_{ads}[C_{metal}]}{1 + K_{ads}[C_{metal}]}\right) \tag{5}$$

dx.doi.org/10.1021/jp410298e | J. Phys. Chem. B 2014, 118, 7739−7749

Here, K_{ads} is the equilibrium binding constant, and C_{metal} is the bulk metal concentration. Combining eqs 4 and 5 yields an expression for the SHG signal intensity as a function of bulk metal concentration (eq 6).

$$|E_{SHG}| \propto A + B' \sinh^{-1}\left[\left(\sigma_0 + \sigma_m\left(\frac{K[C_{metal}]}{1 + K[C_{metal}]}\right)\right)\frac{30.2\ M^{1/2}\ m^2\ C^{-1}}{\sqrt{C_{elec}}}\right] \quad (6)$$

In this expression, constants have been grouped into a single constant B′. Equation 6 is used to fit Mg^{2+} adsorption isotherms at a given constant ionic strength and pH to determine thermodynamic adsorption parameters such as the free energy of adsorption and the surface coverage. Specifically, the methods outlined in this section will be used to compare the initial surface charge densities and thermodynamic binding parameters for Mg(II) adsorption at the solid/water interfaces for bare fused silica, pristine single layer graphene/fused silica, and defected graphene/fused silica.

III. EXPERIMENTAL SECTION

A. Substrate and Solution Preparation. The graphene films were grown by chemical vapor deposition following two different procedures. The preparation and transfer of the first set of CVD graphene samples has been described in detail previously.[59] Briefly, these graphene films were produced using a mixture of H_2, CH_4, and Ar gases under ambient pressure.[59] The second set of graphene samples, named defected graphene, were produced with a mixture of H_2 and CH_4 under low pressure. A more detailed description of this preparation method is available in the Supporting Information. These two procedures produced cm^2-scale graphene films which were then transferred onto the fused silica windows (ISP Optics, 1″ diameter, QI-W-25-1).

For all charge screening and Mg(II) adsorption experiments, fused silica windows (ISP Optics, 1″ diameter, QI-W-25-1) were used along with fused silica hemispheres (ISP Optics, 1″ diameter, QU-HS-25). The silica hemispheres were cleaned prior to every experiment as follows: they were treated with a NoChromix solution (Godax Laboratories) for 1 h, rinsed with Millipore water (18.2 MΩ), sonicated in methanol for 6 min, dried in a 110 °C oven for 30 min, and finally oxygen plasma cleaned (Harric Plasma) on the highest setting for 30 s before being stored in Millipore water for later use. The graphene samples were not treated with NoChromix, and were instead cleaned by flushing with 2 L of Millipore water before and after each experiment. Solutions of NaCl and Mg(II) were prepared in Millipore water using NaCl (Alfa Aesar, 99+%) and $MgCl_2 \cdot 6H_2O$ (Sigma-Aldrich, 99.0%). During the duration of each experiment, the aqueous solutions were maintained at pH 7 with dilute solutions of ∼1 M NaOH (Sigma-Aldrich, 99.99%) and HCl (EMD ACS grade).

B. Raman Analysis. Raman spectra were recorded with an Acton TriVista CRS Confocal Raman System. Spectra were collected using an excitation wavelength of 514.5 nm with a 100× objective at a power density $<10^6$ W/cm^2 to avoid sample damage. Raman analyses were used to confirm the presence of single layer graphene, to assess their defect densities, and to test whether the samples were altered as a result of SHG experimental procedures.

C. Laser and Detection System. A detailed description of the SHG setup used here is available elsewhere.[53,70,87,88] Briefly, a regeneratively amplified Ti:Sapphire system (Hurricane, Spectra Physics) running at a 1 kHz repetition rate pumps an optical parametric amplifier (OPA-CF, Spectra-Physics), which is tuned to a fundamental frequency between 597 and 610 nm, where this particular system exhibits maximum power stability. Using a variable density filter, the pulse energy measured before the fused silica hemisphere is attenuated to 0.09 ± 0.02 μJ/pulse. After passing through the fused silica hemisphere, this pulse energy equates to a power density of approximately 10(3) × 10^4 μJ/cm^2 per pulse for a 30 μm focal spot. This condition was maintained so that experiments are run well below the graphene damage threshold, as reported previously.[59] This reported laser fluence is also below the 14 mJ/cm^2 laser damage threshold reported by Currie et al. and other reports that determined graphene damage thresholds.[89−94] The beam is then directed through the silica hemisphere and silica window so that it is focused at the water/graphene/silica interface at an angle below the total internal reflection. The output light, which is composed of the reflected fundamental light at frequency ω and the second harmonic signal at frequency 2ω, is directed through the Schott filter to remove any contribution at the fundamental light frequency. The second harmonic signal is then directed into a monochromator set at 2ω, passes into a PMT where the electronic signal is amplified, and finally collected using a gated single-photon counting system.[53,70,87,88]

D. Flow System. All of the SHG experiments were carried out under the flow conditions as previously published.[59] A schematic of the custom built flow cell is shown in Figure 1 for clarity. The graphene film is placed face down over a Viton O-ring such that the graphene film is in contact with the aqueous phase. The silica hemisphere is then clamped over the sample window with a layer of Millipore water sandwiched in between to minimize the change of refractive index between the hemisphere and window materials while avoiding the use of an index-matched fluid for reasons of contamination. A ring of water is maintained around the window to prevent evaporation of the sandwiched water layer over the duration of the experiment. Two peristaltic pumps draw solutions from two different reservoirs at flow rates of ∼0.9 mL/s using a flow meter. For charge screening experiments, two reservoirs held the stock pH 7 Millipore water and the salt solution adjusted to pH 7. NaCl concentrations were verified with a conductivity meter (Fisher Traceable Conductivity and TDS meter, Fisher Scientific). For Mg^{2+} adsorption experiments, the reservoirs held the stock Millipore water solution adjusted to pH 7 and

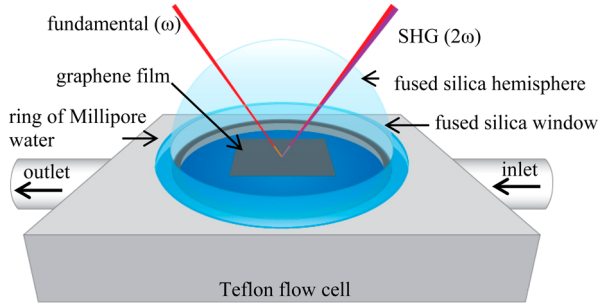

Figure 1. Schematic of the Teflon cell experimental setup showing the relative scale of the graphene film compared to the silica window, and the general position of the focused beam.

dx.doi.org/10.1021/jp410298e | J. Phys. Chem. B 2014, 118, 7739−7749

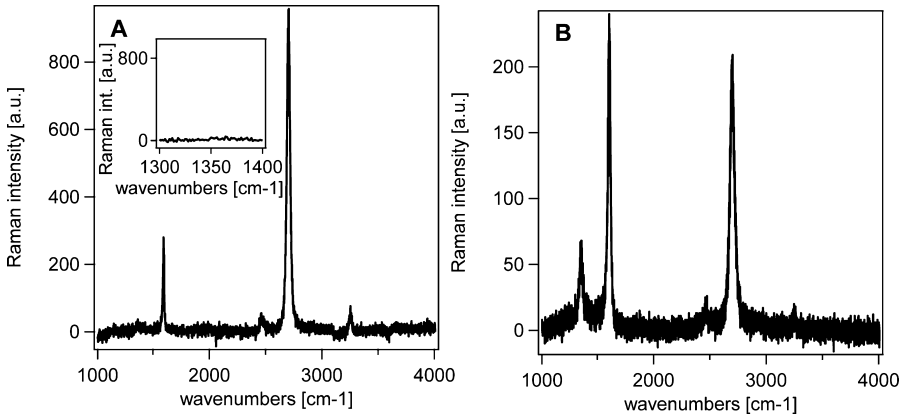

Figure 2. Representative Raman spectra of (A) graphene prepared at ambient pressure and (B) graphene prepared at low pressure after transfer to the fused silica substrates. Inset: Signal to noise level in the 1350 cm^{-1} region for the ambient pressure graphene sample.

the Mg(II) solution at pH 7, both with a 10 mM NaCl background electrolyte concentration. Exact Mg(II) concentrations were determined through a collection of aliquots from each Mg(II) solution used in the SHG experiments that were analyzed with inductively coupled plasma atomic emission spectroscopy (ICP-AES, Varian).

Control studies outlined in our previous publication[59] have shown that the SHG response is well polarized, and that running the experiments at or below 0.15 μJ of input pulse energy avoids sample damage and any contributions from nonlinear optical processes other than SHG. We also used Raman and UV−vis spectroscopies to confirm that the graphene films were not altered as a consequence of the experimental conditions, including aqueous flow and ionic strength. These results are available in the Supporting Information and in our previous publication.[59]

Utilizing our dual-pump flow system, adsorption−desorption traces are recorded as follows: a background stock solution is flowed over the graphene film on the silica substrate for a minimum of 7 min. Once the SHG signal becomes level, steady state conditions are assumed. At this point the flow is stopped, and flow from the second reservoir containing the desired Mg(II) concentration is started. We emphasize here that the background electrolyte concentration and pH are maintained constant and monitored prior to each switch between flow of the background electrolyte solution or the Mg(II) solution. Again the SHG signal is monitored, and after several minutes, once the steady-state signal level is reached, the flow of the Mg(II) solution is stopped, and the system is again flushed with the background stock solution. Here the SHG response increases back to the original level and signal collection continues until steady-state is reached.

IV. RESULTS AND DISCUSSION

A. Raman Spectroscopy of Defect-Free and Defected Graphene Samples. Raman spectroscopy is commonly used to accurately determine the number of graphene layers between 1 and 5 sheets.[95] Raman spectra of graphene are generally dominated by three bands; a G peak at 1580 cm^{-1}, a 2D peak at 2700 cm^{-1}, and sometimes a D peak at 1350 cm^{-1}.[95−97] The G and 2D bands are attributed to the E_{2g} phonon at the Brillouin zone center and the in-plane transverse optical phonons in the highest optical branch near K, respectively.[95−98] The ratio of the intensity of the G and 2D bands, $I(G)/I(2D)$, and the shape and FWHM of the 2D band can be used to determine the number of graphene layers.[29,95,97,99−102] The D band is due to the breathing modes of six-atom rings of A_{1g} symmetry and is only activated in the presence of defects and can thus be used as a relative identifier of the abundance of defects within a graphene film.[96,98,103] Due to the two different procedures used to produce the graphene films, we were able to analyze graphene films both with and without this characteristic D band. Figure 2 shows representative Raman spectra for both the ambient pressure graphene samples and the low-pressure graphene samples.

Graphene films prepared under ambient pressure exhibited a G:2D band ratio of 0.35(6) and a monomodal 2D band with a 35(1) cm^{-1} FWHW measured over 2 spots, indicative of single layer graphene.[29,95,97,99−102] The number in parentheses is the standard error on the point estimate. Additionally, due to the absence of a D band, the graphene films produced under ambient pressure can be clearly classified as single layer graphene sheets with high crystallinity and a low defect density. However to be comprehensive, as discussed in the Supporting Information, we follow Cançado et al. to estimate an upper bound for the point defect density of the graphene films produced under ambient pressure.[96] Given the signal-to-noise ratio in the Raman spectra for the pristine graphene film (inset Figure 2A), one may estimate an upper bound for the number of defects present as 7.8×10^9 defects per cm^2, corresponding to a distance between defects of 64 nm. We emphasize that these are upper limit estimates at most, since the Raman signal intensity at 1350 cm^{-1} is in fact not above the noise. In comparison to the graphene films prepared under ambient pressure, the graphene films produced with the low pressure method exhibited a D band in the Raman spectra around 1350 cm^{-1}, indicative of the presence of defects. A detailed Raman analysis of the graphene films prepared with the low pressure method is available in the Supporting Information.

B. Initial Surface Charge Density. We have reported previously that pristine single layer graphene on fused silica prepared with the ambient pressure method is found to have an effective surface charge density of −0.0049(8) C/m^2 when compared to the measured surface charge density of bare fused silica at −0.013(6) C/m^2.[53,56,59] We concluded that the graphene sheet effectively screens the silica surface charges or reduces the interfacial charge density of the silica by 60%.[59] In order to compare Mg^{2+} ion adsorption over defect-free and defected graphene it was necessary to determine whether the presence of defects in the graphene sheet significantly altered

dx.doi.org/10.1021/jp410298e | J. Phys. Chem. B 2014, 118, 7739−7749

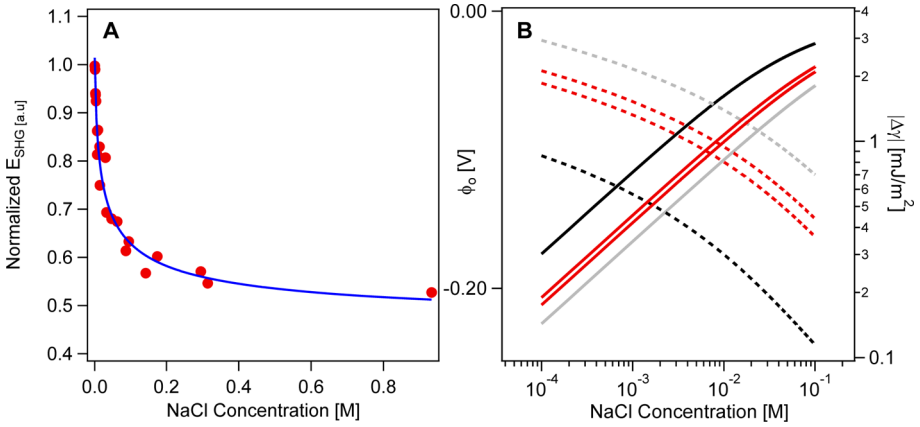

Figure 3. (A) SHG response as a function of NaCl concentration at pH 7. The blue line represents the modified Gouy−Chapman fit using D and K fit parameters corresponding to pristine graphene. (B) Calculated interfacial potentials (solid lines) and absolute free energy density (dashed lines) for bare fused silica (gray) and pristine single layer graphene (black) as shown in ref 56. Appended are the range of results for defected graphene (red) as a function of NaCl concentration at pH7 with calculated interfacial charge densities of −0.009(3) and −0.010(3) C/m^2.

the effective initial surface charge density. To this end, we carried out a charge screening experiment at pH 7 using methods described previously.[53,59,64,86] Briefly, we collected the I_{SHG} as a function of NaCl concentration up to 0.4 M at pH 7. SHG intensity normalization, referencing, and averaging was carried out on data obtained from triplicate measurements as described previously.[59] The screening experiments were repeated on separate days and over the same defected graphene sample. The normalized E_{SHG} field is plotted as a function of NaCl concentration and fit with the modified Gouy−Chapman fit as shown in Figure 3.

To determine the interfacial charge density, the salt screening data was fit to the modified Gouy−Chapman model proposed in our previous work.[59] This modified model is similar to eq 4 except for an additional term describing the buildup of the electrical double layer at lower salt concentrations, according to

$$E_{SHG} = A + B^* \operatorname{arcsinh}\left[\sigma_0^*\left(\frac{30.2\ \mathrm{M}^{1/2}\ \mathrm{m}^2\ \mathrm{C}^{-2}}{\sqrt{C_{elec}}}\right)\right] + D\left(\frac{KC_{elec}}{1 + KC_{elec}}\right) \quad (7)$$

Here, D is a unitless scaling parameter, C_{elec} is the electrolyte concentration, and K is the observed equilibrium constant for establishing the electrical double layer, which we reported to be completely formed at electrolyte concentration below 1 mM. The SHG responses at salt concentrations below 1 mM were not collected over the defected graphene samples studied in this present work and as such the electrical double layer was already established. However, use of eq 7 as a fit function facilitates comparison of the results with those we previously reported for fused silica in the presence and absence of pristine single layer graphene.[59] In our present work, the defected graphene charge screening data was fit separately with the D and K values obtained for bare fused silica and pristine graphene,[59] resulting in initial surface charge densities ranging from −0.009(3) to −0.010(3) C/m^2 for the defected graphene. By comparison, we find that the surface charge density of the defected graphene prepared under low pressure is between that of the pristine graphene (−0.0049(8) C/m^2) and bare fused silica (−0.013(6) C/m^2). The defected graphene effectively shields the surface charge of the bare silica window between 23 and 30%.

With the $\chi^{(3)}$ technique, we track the interfacial potential and determine the surface charge density, which can be used together to assess the driving force for adsorption as quantified by the interfacial free energy or surface tension. Using the Lippmann equation,[104] the change in the interfacial free energy density ($\Delta\gamma$) for defected graphene exposed to high versus low ionic strength conditions can be compared to that of pristine graphene and bare fused silica, according to

$$\Delta\gamma = -\sigma\Delta\Phi \quad (8)$$

Here, σ is the initial interfacial charge density determined from the charge screening experiments, and $\Delta\Phi$ is the change in the interfacial potential calculated from the Gouy−Chapman model for various ionic strengths, as shown in eq 4. In our past work,[59] the presence of a single layer of pristine graphene reduced the interfacial free energy density by a factor of 7. Here, in the case of the defected graphene, the interfacial free energy density at the silica/water interface is only reduced by a factor up to 2. While there is a subtle change of the interfacial charge density between graphene and defected graphene, it appears that the presence of defects in the graphene sheet, which we estimate here to be around 1.3×10^{11} defects per cm^2, only minimally reduces the interfacial free energy density from that of bare fused silica.

C. Mg(II) Adsorption/Desorption Traces. To assess whether a divalent metal ion such as Mg(II) interacts more or less strongly with single layer graphene in the presence or absence of defects, adsorption/desorption studies were performed using Mg(II) solutions maintained at pH 7, under a constant flow of 0.9 mL/sec, and with a 10 mM background NaCl concentration. Adsorption/desorption traces are shown in Figure 4. These traces are obtained by taking the square root of the SHG signal intensity and then normalizing to the water baseline. The baseline is the square root of the averaged Millipore SHG signal before and after each flow of the metal analyte. The decrease of the SHG signal is rationalized by the $\chi^{(3)}$ effect described in eqs 2 and 6, whereby the Mg^{2+} cations are screening the negatively charged surface species, thereby reducing the interfacial potential resulting in a decrease in the SHG E-field at pH 7. As shown in Figure 4 the SHG E-field returns back to the baseline water level upon several minutes of

dx.doi.org/10.1021/jp410298e | J. Phys. Chem. B 2014, 118, 7739−7749

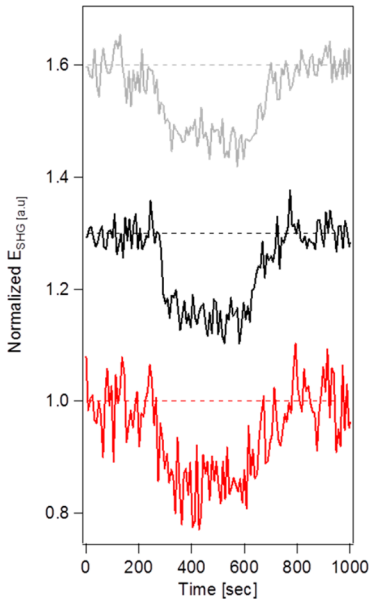

Figure 4. SHG response versus time traces of Mg(II) adsorption/desorption at pH 7 on bare fused silica (black), pristine graphene prepared with the ambient pressure method (gray) and defected graphene prepared with the low pressure method (red). All experiments were performed in the presence of 10 mM NaCl as a background electrolyte and all metal concentrations are ~1 mM of Mg(II). The trace begins with a flow of the background NaCl solution which is then switched to a flow of the Mg(II) solution at approximately 250 s, and finally flushed again with the background NaCl solution at 600 s. The dotted lines represent the background water signal level used for normalization. The three traces are offset for clarity.

flushing with the Millipore stock solution. This return to baseline occurs in all three systems, indicating that Mg(II) ion adsorption is fully reversible for both the silica and the graphene interfaces.

In addition, the duration of the adsorption and desorption processes does not appear to increase or slowdown in the presence of a single layer of graphene. This finding suggests that the mechanism of Mg(II) ion adsorption in the presence of graphene does not involve Mg(II) ion diffusion under the edges of the graphene sheet in order to allow for adsorption at the silica interface. The graphene films used for our studies are on average 1 cm in length and width, and our SHG signal is collected from the approximate center of the film. Taking an extreme case, if we assume that our SHG signal is originating 0.2 cm from the edge of the graphene sheet, based on the diffusion coefficient of a Mg(II) ion in water,[105] it would take approximately 10−40 min for the Mg(II) ion to travel this distance underneath the graphene film. Given that the adsorption/desorption process over the graphene sheet reaches steady-state with tens of seconds, we can discount the possibility that Mg(II) diffusion underneath the graphene sheet is responsible for the observed SHG response. Moreover, the SHG E-field is observed to return to the original water baseline upon flushing with Millipore stock solution, indicating that there is no memory effect. We conclude that it is unlikely that Mg(II) ions are diffusing underneath the graphene sheet. This rationale is supported by a study by Bunch et al., who concluded that edges of graphene sheets suspended over SiO_2 are effectively "clamped down" by van der Waal interactions between the graphene and SiO_2, creating an impermeable membrane.[106]

Another possibility for the apparent Mg(II) transparency of graphene is metal ion diffusion through the graphene layer. Such a transfer process has been reported by Nair et al., who determined graphene oxide multilayers to be impermeable to various liquids and gases, including He,[107] unless conditions with a particular layer and domain spacing parameters were met. In contrast to the Nair et al. work, our Mg(II) ions binding study is carried out on pristine single layer graphene, as well as defected graphene, and not graphene oxide multilayers. Moreover, the barrier for diffusion through graphene of an aquated Mg(II) ion, with its weak polarizability and strongly held hydration sphere, is likely to be high. We conclude that it is unlikely that Mg(II) ions are diffusing through the graphene sheet during the duration of the experiment in the case of pristine graphene. The finding that the results are qualitatively identical for defected graphene suggests that the defected graphene samples are impermeable to Mg(II) ions as well.

D. Mg(II) Adsorption Isotherms. Adsorption isotherms were performed following the adsorption/desorption process described above by collecting the SHG response at 300 nm over a range of Mg(II) concentrations, at pH 7, and with 10

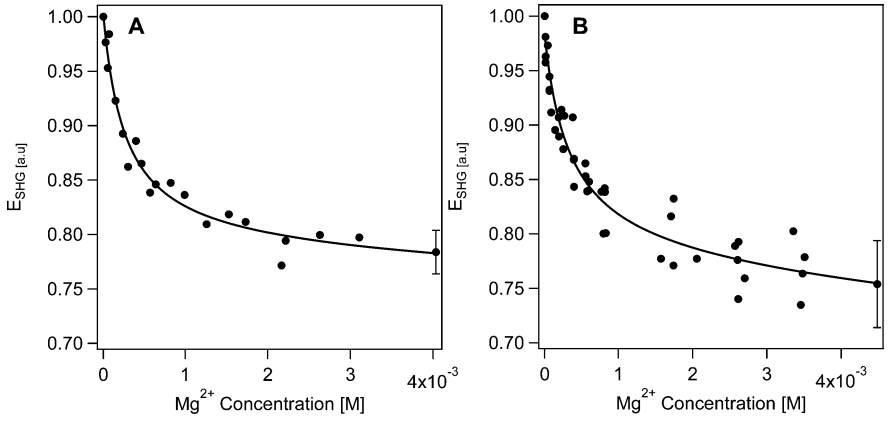

Figure 5. SHG response as a function of Mg(II) concentration at the (A) water/ pristine graphene/fused silica interface and at the (B) water/defected graphene/fused silica interface. All isotherms were performed at pH 7 in the presence of 10 mM NaCl. The solid lines represents the fits to the Langmuir modified Gouy−Chapman model as expressed in eq 6 for a 1:1 symmetric electrolyte. The fit shown in B included an initial surface charge density of 0.009 C/m^2.

dx.doi.org/10.1021/jp410298e | J. Phys. Chem. B 2014, 118, 7739−7749

Table 1. Summary of Binding Parameters for Magnesium to the Fused Silica, Pristine Graphene, and Defected Graphene Interface at pH 7, 10 mM NaCl(aq), and 298 K

sample	initial surface charge density ($-C/m^2$)	$-\Delta G_{ads}$ (kJ/mol)	K_{ads} (M^{-1})	adsorbate number density (ions/cm^2)
silica[a,b]	0.013(6)	30(+1/−3)−30.5(7)	3(2)−4(1) × 10^3	2(1) − 4(1) × 10^{12}
pristine graphene[b,c]	0.0049(8)	30.4(9)−31.1(7)	4(1)−5(1) × 10^3	1.1(5)−- 1.5(4) × 10^{12}
defected graphene[c]	0.009(3)−0.010(3)	30(1)−30.8(6)	3(1)−4(1) x10^3	2(1) − 3.1(5) × 10^{12}

[a]Thermodynamic parameters for magnesium taken from ref 56. [b]Surface charge densities taken from from ref 59. [c]Thermodynamic parameters are given as a range, calculated with a 0.009 and 0.10 C/m^2 initial charge densities, and assuming both a 1:1 and 2:2 electrolyte.

mM NaCl background electrolyte concentration. The Mg(II) adsorption experiments were repeated a total of three times at the pristine graphene/fused silica interface and a total of five times at the defected graphene/fused silica interface. We plot the normalized SHG E-field as a function of bulk Mg(II) concentration in Figure 5. As with the adsorption/desorption studies, the SHG E-field decreases with increasing Mg(II) concentration due to a decrease of the interfacial potential upon Mg(II) adsorption at constant ionic strength. We have shown before, in NaCl control studies, that adding enough NaCl to match the maximum ionic strength of the divalent metal ion analyte results in a minimal decrease of the SHG E-field as compared to the metal analyte alone.[53,69] For this reason we are confident that the observed SHG response is due to the divalent metal interaction with the interface, and is not a consequence of increased ionic strength alone.

In order to obtain quantitative thermodynamic binding parameters for Mg(II) adsorption we fit the binding curves with the Gouy−Chapman model as expressed by eq 6. The initial surface charge densities determined earlier for the pristine graphene (−0.0049(8) C/m^2) and defected graphene (between −0.009(3) and −0.010(3) C/m^2) were used to help constrain the fit. As we have noted previously,[56,69] the Gouy−Chapman model assumes a symmetric (1:1 or 2:2) analyte, which does not match our system of mixed monovalent and divalent electrolytes. While an expression for relating the interfacial potential to a 2:1:1 electrolyte solution has been derived, we are prevented from using this derivation as it cannot be expressed in a closed form for substitution into eq 2. Instead we fit the binding curves in two forms: the first assuming a 1:1 electrolyte solution, and the second assuming a 2:2 electrolyte solution. This approach effectively will underestimate and overestimate the change in the SHG E-field, providing a range of thermodynamic binding parameters for Mg(II) adsorption, as described earlier.[56] The binding curves in Figure 5 are fit assuming a 1:1 electrolyte, and the expression for C_{elec} in eq 6 is set as 0.01 + [M], where M is the concentration of Mg(II) and 0.01 is the addition of the 10 mM background NaCl concentration. This approach assumes that $MgCl_2$ dissociates only to $MgCl^+$. The fit assuming a 2:2 electrolyte is achieved by setting the expression for C_{elec} as equal to [M] alone, which is identical to assuming that all charge screening is due to Mg^{2+} alone with negligible contributions from the screening electrolyte. This fit is not shown in Figure 5, but is included for calculating the range of thermodynamic parameters that are reported in Table 1. Figure 5A shows the Gouy−Chapman fit obtained for two separate sets of Mg(II) adsorption experiments. A third data set was collected and resulted in a qualitatively similar form, but was characterized by more scatter in the data and resulted in a fit of poor quality, so it was not included in the subsequent analysis.

The Gouy−Chapman fit resulted in an observed binding constant, K_{ads}, of 4(1)−5(1) × 10^3 M^{-1} for pristine graphene, and 3(1)−4(1) × 10^3 M^{-1} for defected graphene. Determining the observed binding constant for a series of ionic strengths yields the Coulombic contribution to the free energy of binding and, separately, the non-Coulombic term,[66] which is beyond the scope of the work presented here. With the observed binding constants, free energies of adsorption, referenced to a 55.5 M aqueous solution, were calculated for both graphene films. An adsorption free energy, ΔG_{ads}, for pristine graphene ranged between −30.4(9) and −31.1(7) kJ/mol and for defected graphene ranged between −30(1) and −30.8(6) kJ/mol. A maximum adsorbate charge density was also obtained from the fit and found to range from 0.004(2) to 0.005(1) C/m^2 and from 0.005(3) to 0.010(2) C/m^2 for the pristine and defected graphene, respectively. From the absolute charge density the number of adsorbates can be determined, resulting in 1.1(5)−1.5(4) × 10^{12} ions/cm^2 for pristine graphene, and 2(1)−3.1(5) × 10^{12} ions/cm^2 for defected graphene, assuming the magnesium ions are bound as divalent species. When compared to the pristine single layer graphene, the population of defects within the defected graphene film does not appear to significantly alter the Mg(II) ion surface coverage, at least within our detection limit of 6 × 10^9 alkaline earth metal ions/cm^2.[56] We conclude that all three interfaces studied here have a low density of bound Mg(II) ions. A summary of the previously published results over bare fused silica[56] and the current results from the pristine and defected graphene is presented in Table 1.

The thermodynamic binding parameters presented here for Mg(II) interaction with water/graphene/silica interfaces are in general agreement with the notion that divalent cations interact poorly (binding constants on the order of mM^{-1} were reported for Pb^{2+} interaction with coconut shell activated carbon)[108] with graphene unless the surfaces are heavily modified using, for instance, organic acids,[109] or unless altogether different graphene-based materials, such as graphene oxide, are used.[110] DFT studies regarding the interaction of Mg^{2+} with graphene[20,26] resulted in a height of the adsorbed metal ions of 2−4 Å above the graphene surface and a weak interaction energy (we note, though, that this calculation was carried out in the absence of water). This computational prediction appears to be confirmed by our experimental data. More recently, molecular dynamics simulations by Chialvo and Cummings, which include explicit water molecules, have shown around 4 × 10^{11} Ba^{2+} ions adsorbed per cm^2 within in the first 7 Å from the graphene plane, and around 1.8 × 10^{12} Ba^{2+} ions adsorbed per cm^2 within in the first 13 Å away from the graphene plane.[111] These results are comparable to what we report here from our SHG experiments for the case of Mg(II).

V. CONCLUSION

The SHG $\chi^{(3)}$ method was used to investigate magnesium adsorption at the water/graphene interface both with and without the presence of defects. These results were compared

dx.doi.org/10.1021/jp410298e | J. Phys. Chem. B 2014, 118, 7739−7749

to previous adsorption studies over bare fused silica to determine if the binding parameters for Mg(II) adsorption were significantly altered due to the presence of a single layer graphene film in between the water and silica phase. With ambient pressure and low pressure CVD methods, we produced highly uniform single layer defect-free and low defect-density graphene films, as confirmed with Raman spectroscopic analyses. The presence of defects within the graphene film prepared with the low pressure method resulted in an initial surface charge density ranging between −0.009(3) and −0.010(3) C/m^2, an approximate 50% increase from that of the pristine single layer graphene. Magnesium adsorption/desorption was found to be fully reversible over the pristine and defected graphene films and occurred on the same time scale as that of bare fused silica, indicating that Mg(II) diffusion underneath the graphene film is highly unlikely. Within our detection limit, the adsorption free energies over both graphene films were quantified to be comparable to that of bare fused silica. The magnitude of the free energies, 30(1)−31.1(7) kJ/mol, is consistent with one or two hydrogen bonds. The absolute number densities of magnesium ions at the pristine graphene and defected graphene/water interfaces were determined to be 1.1(5)−1.5(4) × 10^{12} ions/cm^2 and 2(1)−3.1(5) × 10^{12} ions/cm^2, respectively. The number density at the pristine graphene interface is only minimally smaller than that of bare fused silica, while the number density of the defected graphene is closer to that of bare fused silica, suggesting that the presence or absence of defects in this scale does not significantly affect magnesium adsorption. Through our adsorption studies, we have shown that Mg(II) adsorption over pristine and defected single layer graphene films is not enhanced, and perhaps at most only minimally impeded, when compared to adsorption over bare fused silica. This indicates that the influence of the underlying substrate dominates the binding mechanism. These results follow previous experiments that clearly indicate that the presence of a single layer of graphene over an oxide surface has a minimal influence on the electrical double layer.[59] These results are also similar to the two-photon photoemission studies carried out on epitaxial graphene on the Ir(111) surface, which determined the image-potential-states minimally changed as a function of graphene coverage.[112] These studies provide an important benchmark for theory calculations and atomistic simulations of the electrical double layer over carbon interfaces. This work clearly demonstrates the versatility of SHG for providing highly sensitive quantitative information on the interactions of ions with carbon substrates and other charged interfaces.

■ ASSOCIATED CONTENT

Ⓢ Supporting Information

Preparation of the low-pressure graphene, Raman analysis of the low-pressure graphene, and Raman and UV−vis control studies. This information is available free of charge via the Internet at http://pubs.acs.org.

■ AUTHOR INFORMATION

Corresponding Author

*E-mail: geigerf@chem.northwestern.edu. Phone: +1-847-467-6553.

Notes

The authors declare no competing financial interest.

■ ACKNOWLEDGMENTS

This work was supported by the Fluid Interface Reactions, Structures and Transport (FIRST) Center, an Energy Frontier Research Center funded by the U.S. Department of Energy, Office of Science, Office of Basic Energy Sciences. This work made use of the Keck-II facility (NUANCE Center - Northwestern University), which has received support from the W. M. Keck Foundation, Northwestern's Institute for Nanotechnology's NSF-sponsored Nanoscale Science & Engineering Center (EEC-0118025/003), both programs of the National Science Foundation, the State of Illinois, and Northwestern University.

■ REFERENCES

(1) Gogotsi, Y. Controlling Graphene Properties through Chemistry. *J. Phys. Chem. Lett.* **2011**, *2* (19), 2509−2510.
(2) Batzill, M. The Surface Science of Graphene: Metal Interfaces, CVD Synthesis, Nanoribbons, Chemical Modifications, and Defects. *Surf. Sci. Rep.* **2012**, *67* (3−4), 83−115.
(3) Brownson, D. A.; Kampouris, D. K.; Banks, C. E. Graphene Electrochemistry; Fundamental Concepts through to Prominent Applications. *Chem. Soc. Rev.* **2012**, *41*, 6944−6976.
(4) Geim, A. K.; Novoselov, K. S. The Rise of Graphene. *Nat. Mater.* **2007**, *6*, 183−191.
(5) Feng, X.; Maier, S.; Salmeron, M. Water Splits Epitaxial Graphene and Intercalates. *J. Am. Chem. Soc.* **2012**, *134* (12), 5662−5668.
(6) Liang, Y.; Wang, H.; Zhou, J.; Li, Y.; Wang, J.; Regier, T.; Dai, H. Covalent Hybrid of Spinel Manganese−Cobalt Oxide and Graphene as Advanced Oxygen Reduction Electrocatalysts. *J. Am. Chem. Soc.* **2012**, *134* (7), 3517−3523.
(7) Guo, F.; Silverberg, G.; Bowers, S.; Kim, S.-P.; Datta, D.; Shenoy, V.; Hurt, R. H. Graphene-Based Environmental Barriers. *Environ. Sci. Technol.* **2012**, *46* (14), 7717−7724.
(8) Ratinac, K. R.; Yang, W.; Ringer, S. P.; Braet, F. Toward Ubiquitous Environmental Gas Sensors—Capitalizing on the Promise of Graphene. *Environ. Sci. Technol.* **2010**, *44* (4), 1167−1176.
(9) Tang, K.; Fu, L.; White, R. J.; Yu, L.; Titirici, M.-M.; Antonietti, M.; Maier, J. Hollow Carbon Nanospheres with Superior Rate Capability for Sodium-Based Batteries. *Adv. Energy Mater.* **2012**, *2* (7), 873−877.
(10) Shu, C.; Wang, E.; Jiang, L.; Sun, G. High Performance Cathode Based on Carbon Fiber Felt for Magnesium−Air Fuel Cells. *Int. J. Hydrogen Energy* **2013**, *38* (14), 5885−5893.
(11) Lee, J.-S.; Lee, T.; Song, H.-K.; Cho, J.; Kim, B.-S. Ionic Liquid Modified Graphene Nanosheets Anchoring Manganese Oxide Nanoparticles as Efficient Electrocatalysts for Zn−Air Batteries. *Energy Environ. Sci.* **2011**, *4* (10), 4148−4154.
(12) Dubacheva, G. V.; Liang, C.-K.; Bassani, D. M. Functional Monolayers from Carbon Nanostructures − Fullerenes, Carbon Nanotubes, and Graphene − as Novel Materials for Solar Energy Conversion. *Coord. Chem. Rev.* **2012**, *256* (21−22), 2628−2639.
(13) Guo, S.; Dong, S. Graphene Nanosheet: Synthesis, Molecular Engineering, Thin Film, Hybrids, and Energy and Analytical Applications. *Chem. Soc. Rev.* **2011**, *40* (5), 2644−2672.
(14) Singh, V.; Joung, D.; Zhai, L.; Das, S.; Khondaker, S. I.; Seal, S. Graphene Based Materials: Past, Present and Future. *Prog. Mater Sci.* **2011**, *56* (8), 1178−1271.
(15) Sahin, H.; Peeters, F. M. Adsorption of Alkali, Alkaline-Earth, and 3d Transition Metal Atoms on Silicene. *Phys. Rev. B* **2013**, *87* (8), 085423.
(16) Caragiu, M.; Finberg, S. Alkali Metal Adsorption on Graphite: A Review. *J. Phys.: Condens. Matter* **2005**, *17*, R995−R1024.
(17) Chialvo, A. A.; Cummings, P. T. Aqua Ions−Graphene Interfacial and Confinement Behavior: Insights from Isobaric−Isothermal Molecular Dynamics. *J. Phys. Chem. A* **2011**, *115* (23), 5918−5927.

(18) Chialvo, A. A.; Simonson, J. M. Molecular Dynamics Simulation of the Interfacial Behavior of Short-Chain Polystyrene Sulfonate Aqueous Solutions in Contact with Graphene Surfaces in the Presence of Multivalent Cations. *J. Phys. Chem. C* **2008**, *112* (49), 19521−19529.
(19) Kalluri, R. K.; Konatham, D.; Striolo, A. Aqueous Nacl Solutions within Charged Carbon-Slit Pores: Partition Coefficients and Density Distributions from Molecular Dynamics Simulations. *J. Phys. Chem. C* **2011**, *115* (28), 13786−13795.
(20) Kato, K.; Iyama, T.; Tachikawa, H. Density Functional Theory Study of the Interaction of Magnesium Ions with Graphene Chip. *Jpn. J. Appl. Phys.* **2011**, *50*, 01BJ01-1−01BJ01-4.
(21) Simon, P.; Gogotsi, Y. Capacitive Energy Storage in Nanostructured Carbon−Electrolyte Systems. *Acc. Chem. Res.* **2012**, *46* (5), 1094−1103.
(22) Gruneis, A. Synthesis and Electrical Properties of Chemically Functionalized Graphene on Metal Surfaces. *J. Phys.: Condens. Matter* **2013**, 25.
(23) Wehling, T. O.; Katsnelson, M. I.; Lichtenstein, A. I. Impurities on Graphene: Midgap States and Migration Barriers. *Phys. Rev. B* **2009**, *80* (8), 085428.
(24) Sreeprasad, T. S.; Berry, V. How Do the Electrical Properties of Graphene Change with Its Functionalization? *Small* **2013**, *9* (3), 341−350.
(25) Gorjizadeh, N.; Farajian, A. A.; Esfarjani, K.; Kawazoe, Y. Spin and Band-Gap Engineering in Doped Graphene Nanoribbons. *Phys. Rev. B* **2008**, *78* (15), 155427.
(26) Chan, K. T.; Neaton, J. B.; Cohen, M. L. First-Principles Study of Metal Adatom Adsorption on Graphene. *Phys. Rev. B* **2008**, *77* (23), 235430.
(27) Chen, J.-H.; Jang, C.; Adam, S.; Fuhrer, M. S.; Williams, E. D.; Ishigami, M. Charged-Impurity Scattering in Graphene. *Nat. Phys.* **2008**, *4*, 377−381.
(28) Wei, D.; Wu, B.; Guo, Y.; Yu, G.; Liu, Y. Controllable Chemical Vapor Deposition Growth of Few Layer Graphene for Electronic Devices. *Acc. Chem. Res.* **2012**, *46* (1), 106−115.
(29) Peltekis, N.; Kumar, S.; McEvoy, N.; Lee, K.; Weidlich, A.; Duesberg, G. S. The Effect of Downstream Plasma Treatments on Graphene Surfaces. *Carbon* **2012**, *50* (2), 395−403.
(30) Dean, J. J.; van Driel, H. M. Second Harmonic Generation from Graphene and Graphitic Films. *Appl. Phys. Lett.* **2009**, *95* (26), 261910.
(31) Dean, J. J.; van Driel, H. M. Graphene and Few-Layer Graphite Probed by Second-Harmonic Generation: Theory and Experiment. *Phys. Rev. B* **2010**, *82* (12), 125411.
(32) Klekachev, A. V.; Asselberghs, I.; Huyghebaert, C.; Vanbel, M.; Van der Veen, M. A.; Stesmans, A. L.; Heyns, M. M.; De Gendt, S.; Verbiest, T. SHG/2PF Microscopy of Single and Multi-Layer Graphene. In *Optical Processes in Organic Materials and Nanostructures*. Proceedings of the SPIE, 2012; pp 847405-1−847405-8.
(33) Bykov, A. Y.; Murzina, T. V.; Rybin, M. G.; Obraztsova, E. D. Second Harmonic Generation in Multilayer Graphene Induced by Direct Electric Current. *Phys. Rev. B* **2012**, *85* (12), 121413.
(34) An, Y. Q.; Nelson, F.; Lee, J. U.; Diebold, A. C. Enhanced Optical Second-Harmonic Generation from the Current-Biased Graphene/SiO_2/Si(001) Structure. *Nano Lett.* **2013**, *13* (5), 2104−2109.
(35) Hong, S.-Y.; Dadap, J. I.; Petrone, N.; Yeh, P.-C.; Hone, J.; Osgood, R. M. Optical Third-Harmonic Generation in Graphene. *Phys. Rev.* **2013**, *3* (2), 021014.
(36) Hendry, E.; Hale, P. J.; Moger, J.; Savchenko, A. K.; Mikhailov, S. A. Coherent Nonlinear Optical Response of Graphene. *Phys. Rev. Lett.* **2010**, *105* (9), 097401.
(37) Gu, T.; Petrone, N.; McMillan, J. F.; van der Zande, A.; Yu, M.; Lo, G. Q.; Kwong, D. L.; Hone, J.; Wong, C. W. Regenerative Oscillation and Four-Wave Mixing in Graphene Optoelectronics. *Nat. Photonics* **2012**, *6* (8), 554−559.
(38) Kumar, S.; Kamaraju, N.; Vasu, K. S.; Sood, A. K. Femtosecond Photoexcited Carrier Dynamics in Reduced Graphene Oxide Suspensions and Films. *Int. J. Nanosci.* **2011**, *10* (4/5), 669−673.
(39) Bao, Q.; Loh, K. P. Graphene Photonics, Plasmonics, and Broadband Optoelectronic Devices. *ACS Nano* **2012**, *6* (5), 3677−3694.
(40) Zhang, H.; Virally, S.; Bao, Q.; Loh, K. P.; Massar, S.; Godbout, N.; Kockaert, P. Z-Scan Measurement of the Nonlinear Refractive Index of Graphene. *Opt. Lett.* **2012**, *37*, 1856−1858.
(41) Eisenthal, K. B. Liquid Interfaces Probed by Second-Harmonic and Sum-Frequency Spectroscopy. *Chem. Rev.* **1996**, *96*, 1343−1360.
(42) Shen, Y. R. *The Principles of Nonlinear Optics*; John Wiley & Sons: New York, 1984.
(43) Boyd, R. W., *Nonlinear Optics*, 3rd ed.; Academic Press: New York, 2003.
(44) Eisenthal, K. B. Second Harmonic Spectroscopy of Aqueous Nano- and Microparticle Interfaces. *Chem. Rev.* **2006**, *106* (4), 1462−1477.
(45) Corn, R. M.; Higgins, D. A. Optical Second Harmonic Generation as a Probe of Surface Chemistry. *Chem. Rev.* **1994**, *94* (1), 107−125.
(46) Xiao, X.-D.; Vogel, V.; Shen, Y. R. Probing the Proton Excess at Interfaces by Second Harmonic Generation. *Chem. Phys. Lett.* **1989**, *163* (6), 555−559.
(47) Yan, E. C. Y.; Liu, Y.; Eisenthal, K. B. New Method for Determination of Surface Potential of Microscopic Particles by Second Harmonic Generation. *J. Phys. Chem. B* **1998**, *102* (33), 6331−6336.
(48) Zhao, X.; Ong, S.; Wang, H.; Eisenthal, K. B. New Method for Determination of Surface pK_a Using Second Harmonic Generation. *Chem. Phys. Lett.* **1993**, *214* (2), 203−207.
(49) Shen, Y. R. *The Principles of Nonlinear Optics*; John Wiley & Sons, Inc.: Hoboken, NJ, 2003.
(50) Jena, K. C.; Covert, P. A.; Hore, D. K. The Effect of Salt on the Water Structure at a Charged Solid Surface: Differentiating Second- and Third-Order Nonlinear Contributions. *J. Phys. Chem. Lett.* **2011**, *2*, 1056−1061.
(51) Ong, S.; Zhao, X.; Eisenthal, K. B. Polarization of Water Molecules at a Charged Interface: Second Harmonic Studies of the Silica/Water Interface. *Chem. Phys. Lett.* **1992**, *191* (3−4), 327−335.
(52) Salafsky, J. S.; Eisenthal, K. B. Protein Adsorption at Interfaces Detected by Second Harmonic Generation. *J. Phys. Chem. B* **2000**, *104* (32), 7752−7755.
(53) Hayes, P. L.; Malin, J. N.; Konek, C. T.; Geiger, F. M. Interaction of Nitrate, Barium, Strontium and Cadmium Ions with Fused Quartz/Water Interfaces Studied by Second Harmonic Generation. *J. Phys. Chem. A* **2008**, *112* (4), 660−668.
(54) Stumm, W.; Morgan, J. J.; *Aquatic Chemistry: Chemical Equilibria and Rates in Natural Waters*; John Wiley & Sons: New York, 1996.
(55) Morel, F. M. M.; Hering, J. G. *Principles and Applications of Aquatic Chemistry*; John Wiley & Sons: New York, 1993.
(56) Hayes, P. L.; Malin, J. N.; Jordan, D. S.; Geiger, F. M. Get Charged Up: Nonlinear Optical Voltammetry for Quantifying the Thermodynamics and Electrostatics of Metal Cations at Aqueous/Oxide Interfaces. *Chem. Phys. Lett.* **2010**, *499* (4−6), 183−192.
(57) Troiano, J. M.; Jordan, D. S.; Hull, C. J.; Geiger, F. M. Interaction of Cr(III) and Cr(VI) with Hematite Studied by Second Harmonic Generation. *J. Phys. Chem. C* **2013**, *117* (10), 5164−5171.
(58) Jordan, D. S.; Hull, C. J.; Troiano, J. M.; Riha, S. C.; Martinson, A. B. F.; Rosso, K. M.; Geiger, F. M. Second Harmonic Generation Studies of Fe(II) Interactions with Hematite (α-Fe_2O_3). *J. Phys. Chem. C* **2013**, *117* (8), 4040−4047.
(59) Achtyl, J. L.; Vlassiouk, I. V.; Fulvio, P. F.; Mahurin, S. M.; Dai, S.; Geiger, F. M. Free Energy Relationships in the Electrical Double Layer over Single-Layer Graphene. *J. Am. Chem. Soc.* **2013**, *135* (3), 979−81.
(60) Chen, E. H.; Saslow, S. A.; Nguyen, S. T.; Geiger, F. M. Zinc Ion−Hydroxyl Interactions at Undecanol-Functionalized Fused Silica/Water Interfaces Using the Eisenthal $\chi^{(3)}$ Technique. *J. Phys. Chem. C* **2012**, *116* (12), 7016−7020.
(61) Jordan, D. S.; Saslow, S. A.; Geiger, F. M. Exponential Sensitivity and Speciation of Al(III), Sc(III), Y(III), La(III), and Gd(III) at Fused

Silica/Water Interfaces. *J. Phys. Chem. A* **2011**, *115* (50), 14438−14445.
(62) Malin, J. N.; Holland, J. G.; Saslow, S. A.; Geiger, F. M. U(Vi) Adsorption and Speciation at the Acidic Silica/Water Interface Studied by Resonant and Nonresonant Second Harmonic Generation. *J. Phys. Chem. C* **2011**, *115* (27), 13353−13360.
(63) Chen, E. H.; Hayes, P. L.; Nguyen, S. T.; Geiger, F. M. Zinc Interactions with Glucosamine-Functionalized Fused Silica/Water Interfaces. *J. Phys. Chem. C* **2010**, *114* (45), 19483−19488.
(64) Jordan, D. S.; Malin, J. N.; Geiger, F. M. Interactions of Al(III), La(III), Gd(III), and Lu(III) with the Fused Silica/Water Interface Studied by Second Harmonic Generation. *Environ. Sci. Technol.* **2010**, *44* (15), 5862−5867.
(65) Malin, J. N.; Geiger, F. M. Uranyl Adsorption and Speciation at the Fused Silica/Water Interface Studied by Resonantly Enhanced Second Harmonic Generation and the $\chi^{(3)}$ Method. *J. Phys. Chem. A* **2010**, *114* (4), 1797−1805.
(66) Malin, J. N.; Holland, J. G.; Geiger, F. M. Free Energy Relationships in the Electric Double Layer and Alkali Earth Speciation at the Fused Silica/Water Interface. *J. Phys. Chem. C* **2009**, *113* (41), 17795−17802.
(67) Hayes, P. L.; Chen, E. H.; Achtyl, J. L.; Geiger, F. M. An Optical Voltmeter for Studying Cetyltrimethylammonium Interacting with Fused Silica/Aqueous Interfaces at High Ionic Strength. *J. Phys. Chem. A* **2009**, *113* (16), 4269−4280.
(68) Gibbs-Davis, J. M.; Kruk, J. J.; Konek, C. T.; Scheidt, K. A.; Geiger, F. M. Jammed Acid−Base Reactions at Interfaces. *J. Am. Chem. Soc.* **2008**, *130* (46), 15444−15447.
(69) Malin, J. N.; Hayes, P. L.; Geiger, F. M. Interactions of Ca, Zn, and Cd Ions at Buried Solid/Water Interfaces Studied by Second Harmonic Generation. *J. Phys. Chem. C* **2009**, *113* (6), 2041−2052.
(70) Musorrafiti, M. J.; Konek, C. T.; Hayes, P. L.; Geiger, F. M. Interaction of Chromium(VI) with the α-Aluminum Oxide−Water Interface. *J. Phys. Chem. C* **2008**, *112* (6), 2032−2039.
(71) Konek, C. T.; Musorrafiti, M. J.; Voges, A. B.; Geiger, F. M. Tracking the Interaction of Transition Metal Ions with Environmental Interfaces Using Second Harmonic Generation. In *Developments in Earth and Environmental Sciences*; Mark, O. B., Douglas, B. K., Eds.; Elsevier: Amsterdam, 2007; Vol. 7, Chapter 4, pp 95−124.
(72) Fitts, J. P.; Shang, X.; Flynn, G. W.; Heinz, T. F.; Eisenthal, K. B. Electrostatic Surface Charge at Aqueous/α-Al_2O_3 Single-Crystal Interfaces as Probed by Optical Second-Harmonic Generation. *J. Phys. Chem. B* **2005**, *109* (16), 7981−7986.
(73) Zhao, X.; Subrahmanyan, S.; Eisenthal, K. B. Determination of pK_a at the Air/Water Interface by Second Harmonic Generation. *Chem. Phys. Lett.* **1990**, *171* (5−6), 558−562.
(74) Walter, S. R.; Young, K. L.; Holland, J. G.; Gieseck, R. L.; Mirkin, C. A.; Geiger, F. M. Counting the Number of Magnesium Ions Bound to the Surface-Immobilized Thymine Oligonucleotides That Comprise Spherical Nucleic Acids. *J. Am. Chem. Soc.* **2013**, *135* (46), 17339−17348.
(75) Walter, S. R.; Geiger, F. M. DNA on Stage: Showcasing Oligonucleotides at Surfaces and Interfaces with Second Harmonic and Vibrational Sum Frequency Generation. *J. Phys. Chem. Lett.* **2010**, *1* (1), 9−15.
(76) Boman, F. C.; Gibbs-Davis, J. M.; Heckman, L. M.; Stepp, B. R.; Nguyen, S. T.; Geiger, F. M. DNA at Aqueous/Solid Interfaces: Chirality-Based Detection via Second Harmonic Generation Activity. *J. Am. Chem. Soc.* **2009**, *131* (2), 844−848.
(77) Boman, F. C.; Musorrafiti, M. J.; Gibbs, J. M.; Stepp, B. R.; Salazar, A. M.; Nguyen, S. B. T.; Geiger, F. M. DNA Single Strands Tethered to Fused Quartz/Water Interfaces Studied by Second Harmonic Generation. *J. Am. Chem. Soc.* **2005**, *127* (44), 15368−15369.
(78) Holland, J. G.; Geiger, F. M. Importance of Length and Sequence Order on Magnesium Binding to Surface-Bound Oligonucleotides Studied by Second Harmonic Generation and Atomic Force Microscopy. *J. Phys. Chem. B* **2012**, *116* (22), 6302−6310.
(79) Holland, J. G.; Jordan, D. S.; Geiger, F. M. Divalent Metal Cation Speciation and Binding to Surface-Bound Oligonucleotide Single Strands Studied by Second Harmonic Generation. *J. Phys. Chem. B* **2011**, *115* (25), 8338−8345.
(80) Doughty, B.; Kazer, S. W.; Eisenthal, K. B. Binding and Cleavage of DNA with the Restriction Enzyme EcoR1 Using Time-Resolved Second Harmonic Generation. *Proc. Natl. Acad. Sci.* **2011**, *108* (50), 19979−19984.
(81) Holland, J. G.; Geiger, F. M. Y(III) Interactions with Guanine Oligonucleotides Covalently Attached to Aqueous/Solid Interfaces. *J. Phys. Chem. B* **2012**, *117* (3), 825−832.
(82) Holland, J. G.; Malin, J. N.; Jordan, D. S.; Geiger, F. M. Specific and Nonspecific Metal Ion−Nucleotide Interactions at Aqueous/Solid Interfaces Functionalized with Adenine, Thymine, Guanine, and Cytosine Oligomers. *J. Am. Chem. Soc.* **2011**, *133* (8), 2567−2570.
(83) Liu, Y.; Yan, E. C. Y.; Zhao, X.; Eisenthal, K. B. Surface Potential of Charged Liposomes Determined by Second Harmonic Generation. *Langmuir* **2001**, *17* (7), 2063−2066.
(84) Atkins, P.; de Paula, J. *Physical Chemistry*, 7th ed.; W.H. Freeman and Company: New York, 2002.
(85) Langmuir, D. *Aqueous Environmental Geochemistry*; Prentice Hall, Inc.: Upper Saddle River, NJ, 1997.
(86) Saslow Gomez, S. A.; Jordan, D. S.; Troiano, J. M.; Geiger, F. M. Uranyl Adsorption at the Muscovite (Mica)/Water Interface Studied by Second Harmonic Generation. *Environ. Sci. Technol.* **2012**, *46* (20), 11154−11161.
(87) Al-Abadleh, H. A.; Mifflin, A. L.; Musorrafiti, M. J.; Geiger, F. M. Kinetic Studies of Chromium (VI) Binding to Carboxylic Acid- and Methyl Ester-Functionalized Silica/Water Interfaces Important in Geochemistry. *J. Phys. Chem. B* **2005**, *109* (35), 16852−16859.
(88) Hayes, P. L.; Gibbs-Davis, J. M.; Musorrafiti, M. J.; Mifflin, A. L.; Scheidt, K. A.; Geiger, F. M. Environmental Biogeochemistry Studied by Second-Harmonic Generation: A Look at the Agricultural Antibiotic Oxytetracycline. *J. Phys. Chem. C* **2007**, *111* (25), 8796−8804.
(89) Currie, M.; Caldwell, J. D.; Bezares, F. J.; Robinson, J.; Anderson, T.; Chun, H.; Tadjer, M. Quantifying Pulsed Laser Induced Damage to Graphene. *Appl. Phys. Lett.* **2011**, *99* (21), 211909.
(90) Zhou, Y.; Bao, Q.; Varghese, B.; Tang, L. A. L.; Tan, C. K.; Sow, C.-H.; Loh, K. P. Microstructuring of Graphene Oxide Nanosheets Using Direct Laser Writing. *Adv. Mater.* **2010**, *22* (1), 67−71.
(91) Sokolowski-Tinten, K.; Kudryashov, S.; Temnov, V.; Bialkowski, J.; Linde, D.; Cavalleri, A.; Jeschke, H. O.; Garcia, M. E.; Bennemann, K. H. Femtosecond Laser-Induced Ablation of Graphite. In *Ultrafast Phenomena XII*, Springer: Berlin/Heidelberg, 2001; Vol. *66*, pp 425−427.
(92) Jeschke, H. O.; Garcia, M. E.; Bennemann, K. H. Theory for the Ultrafast Ablation of Graphite Films. *Phys. Rev. Lett.* **2001**, *87* (1), 015003.
(93) Xing, G.; Guo, H.; Zhang, X.; Sum, T. C.; Huan, C. H. A. The Physics of Ultrafast Saturable Absorption in Graphene. *Opt. Express* **2010**, *18* (5), 4564−4573.
(94) Lenner, M.; Kaplan, A.; Huchon, C.; Palmer, R. E. Ultrafast Laser Ablation of Graphite. *Phys. Rev. B* **2009**, *79* (18), 184105.
(95) Ferrari, A. C.; Meyer, J. C.; Scardaci, V.; Casiraghi, C.; Lasseri, M.; Mauri, F.; Piscanec, S.; Jiang, D.; Novoselov, K. S.; Roth, S.; Geim, A. K. Raman Spectrum of Graphene and Graphene Layers. *Phys. Rev. Lett.* **2006**, *97* (18), 187401.
(96) Cançado, L. G.; Jorio, A.; Ferreira, E. H. M.; Stavale, F.; Achete, C. A.; Capaz, R. B.; Moutinho, M. V. O.; Lombardo, A.; Kulmala, T. S.; Ferrari, A. C. Quantifying Defects in Graphene via Raman Spectroscopy at Different Excitation Energies. *Nano Lett.* **2011**, *11* (8), 3190−3196.
(97) Ferrari, A. C. Raman Spectroscopy of Graphene and Graphite: Disorder, Electron−Phonon Coupling, Doping and Nonadiabatic Effects. *Solid State Commun.* **2007**, *143* (1−2), 47−57.
(98) Choi, K.; Lim, J.; Rani, J. R.; Yoon, H. S.; Oh, J.; Hong, T.; Ha, T.; Park, B. C.; Sim, K. I.; Jun, S. C.; Kim, J. H. Terahertz and Optical

Study of Monolayer Graphene Processed by Plasma Oxidation. *Appl. Phys. Lett.* **2013**, *102* (13), 131901−4.
(99) Graf, D.; Molitor, F.; Ensslin, K.; Stampfer, C.; Jungen, A.; Hierold, C.; Wirtz, L. Spatially Resolved Raman Spectroscopy of Single- and Few-Layer Graphene. *Nano Lett.* **2007**, *7* (2), 238−242.
(100) Rao, C. N. R.; Sood, A. K.; Subrahmanyam, K. S.; Govindaraj, A. Graphene: The New Two-Dimensional Nanomaterial. *Angew. Chem., Int. Ed.* **2009**, *48* (42), 7752−7777.
(101) Pimenta, M. A.; Dresselhaus, G.; Dresselhaus, M. S.; Cancado, L. G.; Jorio, A.; Saito, R. Studying Disorder in Graphite-Based Systems by Raman Spectroscopy. *Phys. Chem. Chem. Phys.* **2007**, *9* (11), 1276−1290.
(102) Malard, L. M.; Pimenta, M. A.; Dresselhaus, G.; Dresselhaus, M. S. Raman Spectroscopy in Graphene. *Physics Reports* **2009**, *473* (5−6), 51−87.
(103) McEvoy, N.; Nolan, H.; Ashok Kumar, N.; Hallam, T.; Duesberg, G. S. Functionalisation of Graphene Surfaces with Downstream Plasma Treatments. *Carbon* **2013**, *54* (0), 283−290.
(104) Adamson, A. W., *Physical Chemistry of Surfaces*, 5th ed.; John Wiley & Sons Inc.: New York, 1990.
(105) Katz, A.; Ben-Yaakov, S. Diffusion of Seawater Ions. Part II. The Role of Activity Coefficients and Ion Pairing. *Mar. Chem.* **1980**, *8* (4), 263−280.
(106) Bunch, J. S.; Verbridge, S. S.; Alden, J. S.; van der Zande, A. M.; Parpia, J. M.; Craighead, H. G.; McEuen, P. L. Impermeable Atomic Membranes from Graphene Sheets. *Nano Lett.* **2008**, *8* (8), 2458−2462.
(107) Nair, R. R.; Wu, H. A.; Jayaram, P. N.; Grigorieva, I. V.; Geim, A. K. Unimpeded Permeation of Water through Helium-Leak-Tight Graphene-Based Membranes. *Science* **2012**, *335* (6067), 442−444.
(108) Machida, M.; Mochimaru, T.; Tatsumoto, H. Lead(II) Adsorption onto the Graphene Layer of Carbonaceous Materials in Aqueous Solution. *Carbon* **2006**, *44*, 2681−2688.
(109) Kong, N.; Huang, X. D.; Cui, L.; Liu, J. Q. Surface Modified Graphene for Heavy Metal Ions Adsorption. *Sci. Adv. Mater.* **2013**, *5*, 1083−1089.
(110) Wang, S.; Sun, H.; Ang, H. M.; Tade, M. O. Adsorptive Remediation of Environmental Pollutants Using Novel Graphene-Based Nanomaterials. *Chem. Eng. J.* **2013**, *226*, 336−347.
(111) Chialvo, A. A.; Cummings, P. T. Aqua Ions Graphene Interfacial and Confinement Behavior: Insights from Isobaric Isothermal Molecular Dynamics. *J. Phys. Chem. A* **2011**, *115*, 5918−5927.
(112) Niesner, D.; Fauster, T.; Dadap, J. I.; Zaki, N.; Knox, K. R.; Yeh, P. C.; Bhandari, R.; Osgood, R. M.; Petrović, M.; Kralj, M. Trapping Surface Electrons on Graphene Layers and Islands. *Phys. Rev. B* **2012**, *85* (8), 081402.